GEOLOGY | THE GEOLOGICAL SOCIETY OF AMERICA®

https://doi.org/10.1130/G46577.1

Manuscript received 30 May 2019
Revised manuscript received 16 August 2019
Manuscript accepted 22 August 2019

Constraining the maximum depth of brittle deformation at slow- and ultraslow-spreading ridges using microseismicity

Ingo Grevemeyer[1], Nicholas W. Hayman[2], Dietrich Lange[1], Christine Peirce[3], Cord Papenberg[1], Harm J.A. Van Avendonk[2], Florian Schmid[1], Laura Gómez de La Peña[1] and Anke Dannowski[1]

[1]GEOMAR Helmholtz Centre of Ocean Research, Wischhofstraße 1-3, 24148 Kiel, Germany
[2]Institute for Geophysics, Jackson School of Geosciences, University of Texas at Austin, 10100 Burnet Road, Austin, Texas 78758, USA
[3]Department of Earth Sciences, University of Durham, South Road, Durham DH1 3LE, UK

ABSTRACT

The depth of earthquakes along mid-ocean ridges is restricted by the relatively thin brittle lithosphere that overlies a hot, upwelling mantle. With decreasing spreading rate, earthquakes may occur deeper in the lithosphere, accommodating strain within a thicker brittle layer. New data from the ultraslow-spreading Mid-Cayman Spreading Center (MCSC) in the Caribbean Sea illustrate that earthquakes occur to 10 km depth below seafloor and, hence, occur deeper than along most other slow-spreading ridges. The MCSC spreads at 15 mm/yr full rate, while a similarly well-studied obliquely opening portion of the Southwest Indian Ridge (SWIR) spreads at an even slower rate of ~8 mm/yr if the obliquity of spreading is considered. The SWIR has previously been proposed to have earthquakes occurring as deep as 32 km, but no shallower than 5 km. These characteristics have been attributed to the combined effect of stable deformation of serpentinized mantle and an extremely deep thermal boundary layer. In the context of our MCSC results, we reanalyze the SWIR data and find a maximum depth of seismicity of 17 km, consistent with compilations of spreading-rate dependence derived from slow- and ultraslow-spreading ridges. Together, the new MCSC data and SWIR reanalysis presented here support the hypothesis that depth-seismicity relationships at mid-ocean ridges are a function of their thermal-mechanical structure as reflected in their spreading rate.

INTRODUCTION

Seismicity is generally restricted to the mechanically strong lithosphere (Chen and Molnar, 1983), which, along mid-ocean ridges (MORs), may extend for several kilometers beneath the seafloor. At depth, increasing temperature eventually results in plastic deformation, defining a brittle-to-plastic transition and the maximum depth of seismic faulting (Searle and Escartin, 2004). The thermal structure of MOR lithosphere, and thus the thickness of the seismogenic zone, are expected to correlate with spreading rate (Morgan and Chen, 1993). Indeed, earthquakes 4.5 in magnitude or larger are absent along ridge segments spreading at fast and intermediate rates, but are observed along slow- and ultraslow-spreading ridges, where they show a deepening with decreasing spreading rate (Huang and Solomon, 1988). However, larger earthquakes are generally rare along MORs, so instead, local microseismicity data offer a means to study the maximum depth of seismic faulting (e.g., Kong et al., 1992; Wolfe et al., 1995; Tilmann et al., 2004; Korger and Schlindwein, 2014).

To gain further insight into the mechanical behavior of ultraslow-spreading lithosphere, we conducted a microseismicity survey of the Mid-Cayman Spreading Center (MCSC), an ultraslow-spreading center in the Caribbean Sea (Fig. 1). To test our MCSC findings, we also reanalyzed microseismicity data from the similarly ultraslow-spreading Southwest Indian Ridge (SWIR) between 13°E and 14°E, where unusually deep hypocenters have been reported (Schlindwein and Schmid, 2016; Schmid and Schlindwein, 2016). Our results provide new insight into the depth dependence of ultraslow-spreading microseismicity and suggest that the unusually deep hypocenters observed at the SWIR result from a processing artifact. We place our results in context using a compilation of previously published microseismicity surveys from the global mid-ocean ridge system to assess worldwide trends.

MID-CAYMAN SPREADING CENTER MICROSEISMICITY

The MCSC accommodates 15 mm/yr of east-west extension between the North American plate and the Caribbean plate (Hayman et al., 2011), with a deep axial valley of up to 5.5 km in depth and corresponding cold mantle potential temperature (Klein and Langmuir, 1987). In April 2015, we deployed 21 short-period and four broadband ocean-bottom seismographs (OBSs) in the axial region of the Cayman Trough (Fig. 1). These OBSs recorded continuously for up to 16 days. Most OBSs were located near the center of the spreading segment around the Mount Dent oceanic core complex at 18°25′N (Hayman et al., 2011), covering the median valley for 60 km along its length. Instrument spacing was 5–7 km, with an additional three OBSs deployed at the segment ends to assess seismicity along the entire 100-km-long MCSC.

We detected 292 earthquakes, an average of ~20 events per day, with moment magnitudes of $0.4 < M_w < 3.2$. These events were located using P-wave and S-wave phase arrival times picked from waveform data (see the GSA Data Repository[1]). Focal parameters were calculated using a probabilistic, nonlinear earthquake location algorithm (Lomax et al., 2000), and travel times were calculated using a one-dimensional velocity-depth profile derived from a seismic

[1]GSA Data Repository item 2019371, a description of methods, Figs. DR1–DR9, and Table DR1, is available online at http://www.geosociety.org/datarepository/2019/, or on request from editing@geosociety.org.

CITATION: Grevemeyer, I., et al., 2019, Constraining the maximum depth of brittle deformation at slow- and ultraslow-spreading ridges using microseismicity: Geology, v. 47, p. , https://doi.org/10.1130/G46577.1

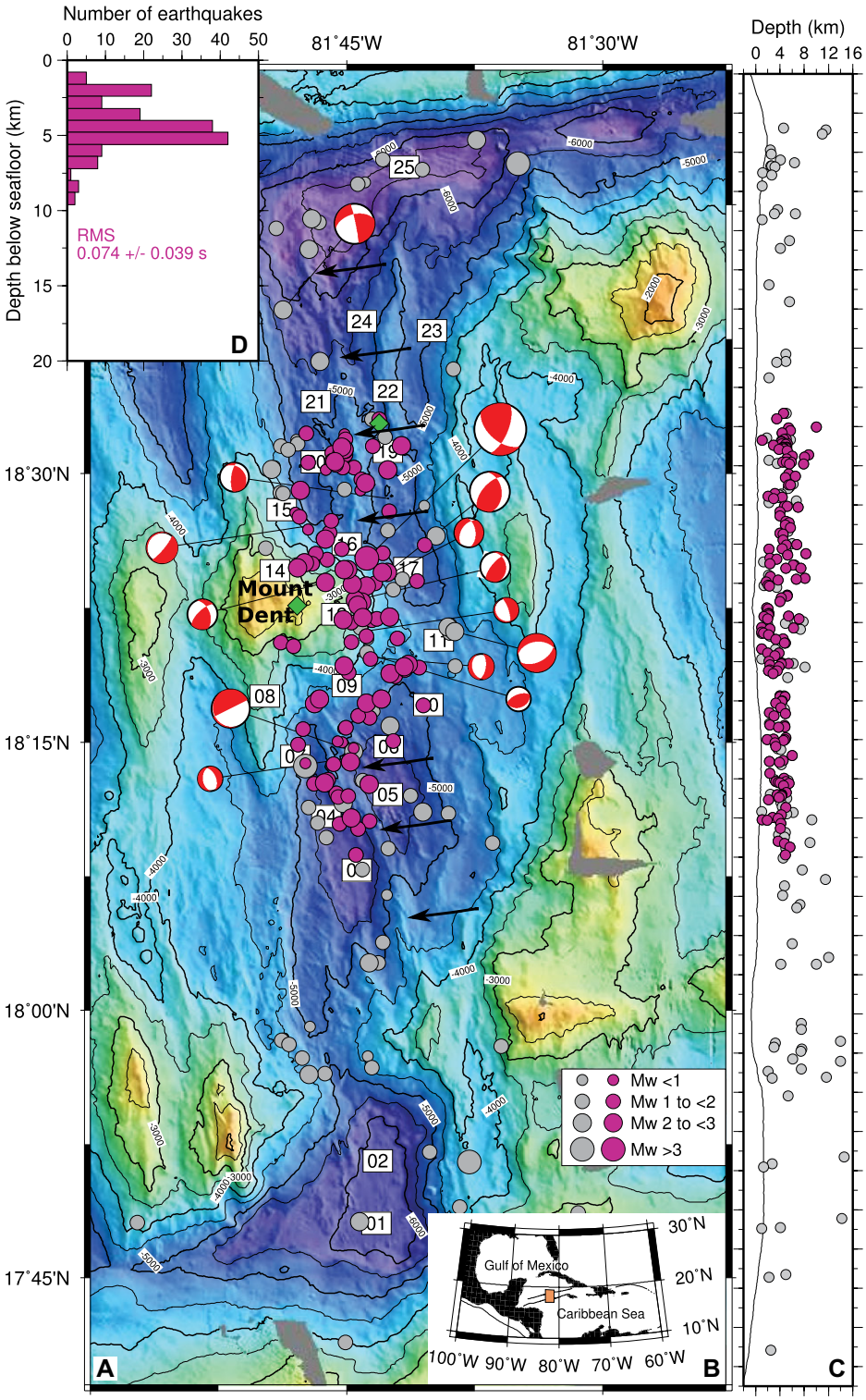

Figure 1. (A) Bathymetric map (contours in meters) of Mid-Cayman Spreading Center (Caribbean Sea) and deployment location of local micro-earthquake monitoring network of ocean-bottom seismographs (OBSs, numbered squares), showing Van Damm and Beebe hydrothermal vents (green diamonds) and epicenters of local seismicity with moment magnitudes of 0.4 < M_w < 3.2 (circles, size scaled to magnitude), where micro-earthquakes recorded at station gap of <180° are colored magenta, and gray circles are events with larger gap. Location of axial volcanic ridge (AVR) is arrowed. Bathymetry is from Grevemeyer et al. (2018b). Focal mechanisms from Table DR1 (see footnote 1) are plotted in red. (B) Map showing geographic context of study area. (C) Micro-earthquakes plotted as function of depth; colors are as in A. (D) Histogram of depth distribution of well-located events (magenta events from A and C). RMS is the root mean square of the travel time residuals from all events in the histogram.

line shot through the seismic network (Van Avendonk et al., 2017). In this model, P-wave velocity (Vp) increases from ~3–4 km/s near the seafloor to 7–8 km/s at 3–5 km depth. The velocity-depth structure as well as geological investigations suggest that volcanic crust occupies most of the axial valley seafloor (Haughton et al., 2019), although exhumed mantle occurs locally (Hayman et al., 2011). S-wave velocity (Vs) was derived using the ratio between P- and S-wave velocity (Vp/Vs), approximated from a cross plot between S-P time and origin time (Fig. DR1 in the Data Repository). This yielded a Vp/Vs ratio of ~1.8 for the uppermost crust (<4 km) and ~1.75 for the mantle. To reduce the impact of non-modeled three-dimensional wave propagation effects, station corrections were calculated and iteratively updated for earthquakes observed by six or more stations that had a station gap of <180°. Station corrections reduced the initial root mean square (RMS) misfit from ~0.12 s to ~0.07 s, and the Gaussian distribution of residuals shows that the resulting station terms are appropriate (Fig. DR2).

Microseismicity clusters at the Mount Dent oceanic core complex (Fig. 1), highlighting the detachment, and along a linear feature interpreted as an axial-volcanic ridge (AVR; Harding et al., 2017). In the south, the AVR, interpreted as a horst by Haughton et al. (2019), traverses the median valley, running obliquely to the overall trend of the MCSC and approaching Mount Dent. To the north, the AVR runs roughly parallel to the trend of the MCSC. Both the Von Damm hydrothermal vent field at Mount Dent and the Beebe vent field to its northeast within the median valley (Connelly et al., 2012) show little seismicity (Fig. 1). However, with an OBS spacing of 5–7 km, this station spacing is likely too large to record small earthquakes caused by thermal cracking (e.g., Sohn et al., 1998).

Well-located earthquakes occur between 4 and 8 km depth, reaching a maximum of 10 km below seafloor (Figs. 1C and 1D; Fig. DR3). The depth of microseismicity also appears to increase toward the segment ends. Most focal mechanisms (Table DR1), derived from P-wave onset first motions, suggest that normal faulting predominates, as might be expected in an extensional tectonic regime. There is evidence for transfer (strike-slip) faulting and compressional earthquakes as well. However, most importantly, the depth range of earthquakes observed at the MCSC is consistent with that expected from the global seismicity temperature-depth relationship.

SWIR OBLIQUE SUPER-SEGMENT MICROSEISMICITY

Schlindwein and Schmid (2016) suggested that, in contrast to the MCSC, the SWIR seismicity pattern is significantly different from that expected from the global temperature-depth

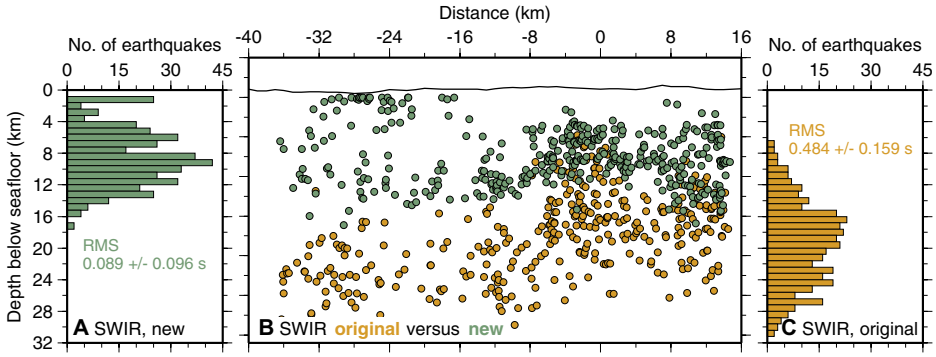

Figure 2. Reanalysis of microseismicity of the Southwest Indian Ridge (SWIR) between 13°E and 14°E (see Fig. DR4 [see footnote 1] for geographic map). (A) Histogram of depth distribution of well-located events (station gap <180°) reanalyzed in this study. (B) Depth distribution along spreading segment; green circles are hypocenters from this study; orange circles are original estimates of Schlindwein and Schmid (2016). (C) Histogram of depth distribution of Schlindwein and Schmid (2016). RMS as in Figure 1.

relationship. The SWIR forms the boundary between the African and Antarctic plates, diverging at an average velocity of 14–16 mm/yr. The area between 13°E and 14°E (Fig. DR4) is part of the so-called oblique super-segment, where the spreading direction is oblique to the trend of the ridge axis (e.g., Dick et al., 2003). In December 2012, ten OBSs were deployed for 1 yr (Schmid and Schlindwein, 2016). Schlindwein and Schmid (2016) analyzed the recorded microseismicity to reveal an aseismic zone in the upper 5–10 km of the lithosphere and unusually deep earthquakes below that, extending to depths of 32 km (Figs. 2B and 2C). This result contradicts the implications of existing thermal-mechanical models of the lithosphere. Here, we test this result against that of the MCSC by reanalyzing the first six months of the deployment when coverage was best.

In our analysis, we adopted the same methodology as applied at the MCSC above. The iterative update of station terms reveals unusually large delays of the S-waves observed at most OBSs, reaching a maximum of 2 s. Any location procedure not accounting for station terms results in biased Wadati diagrams and travel-time residuals (Figs. DR5 and DR6). We believe that the observed large S-wave delays are caused by unconsolidated sediment covering the seafloor; Schmid and Schlindwein (2016) reported deposits of >150 m within the median valley. A 200–400-m-thick layer of unconsolidated, low S-wave velocity, marine sediment of Vs ~200 m/s would cause a delay of 1–2 s. Relocating the events in the catalog and accounting for both P- and S-wave station corrections result in an overall RMS misfit of 0.09 s, more than 4× smaller than the RMS of 0.4 s reported for the original location procedure (Schlindwein and Schmid, 2016). Hypocenters are now located at depths extending from ~1 km to ~17 km below seafloor (Figs. 2A and 2B). In the relocated catalog, neither an aseismic zone in the uppermost lithosphere nor very deep-seated seismicity is revealed.

DISCUSSION

Microseismicity along the MCSC is clearly related to the structure of the median valley, with the majority of earthquakes either wrapping around the Mount Dent core complex, in similar pattern to that observed at other oceanic core complexes (e.g., deMartin et al., 2007; Parnell-Turner et al., 2017), or clustering along the AVR. Some local strike-slip earthquakes appear to reflect oblique kinematics near the associated transform fault segment boundaries. At the MCSC, the region between the seafloor and ~2 km depth is effectively aseismic, similar to results from many studies from the Mid-Atlantic Ridge (MAR) (e.g., Wolfe et al., 1995; Grevemeyer et al., 2013). The deepest micro-earthquakes occur at ~8–10 km below seafloor. This depth is somewhat deeper than observed along most segments of the MAR, but shallower than found along the ultraslow-spreading Gakkel Ridge (Arctic Ocean) (Korger and Schlindwein, 2014), suggesting that micro-earthquakes extend to greater depth as spreading rate decreases (Fig. 3). Such spreading rate–depth relationships for mid-ocean ridge earthquakes are predicted by models that relate the thickness of the brittle lithosphere to its temperature (Morgan and Chen, 1993).

Schlindwein and Schmid's (2016) study of SWIR microseismicity concluded that an extensive aseismic region exists between the seafloor and 5–10 km depth below seafloor, and that such a shallow aseismic regime could result from serpentinization of exhumed mantle, which favors stable sliding on weak faults. However, this interpretation contradicts observations from other settings where serpentinization is pervasive, such as areas affected by subduction-related bend faulting (e.g., Grevemeyer et al., 2018a) or portions of the MAR (e.g., deMartin et al., 2007) where oceanic core complexes exhume deep-seated lithologies to the seafloor.

Microseismicity data from bend-fault settings suggests that serpentinized faults within the mantle are seismically very active and rupture frequently but under low-stress conditions (Lefeldt et al., 2009). At the Rainbow Massif on the MAR, with its high-temperature hydrothermal discharge through ultramafic rocks, micro-earthquakes occur immediately below the vent field and extend to 8–10 km below seafloor (Horning et al., 2018). Similar features were observed at the Logatchev Massif, also on the MAR (Grevemeyer et al., 2013), suggesting that serpentinized domains support elevated levels of seismicity instead of promoting an aseismic regime.

Our new analysis of the SWIR data set indicates that the previously proposed thick aseismic region in the upper lithosphere was simply a consequence of a model embedded in

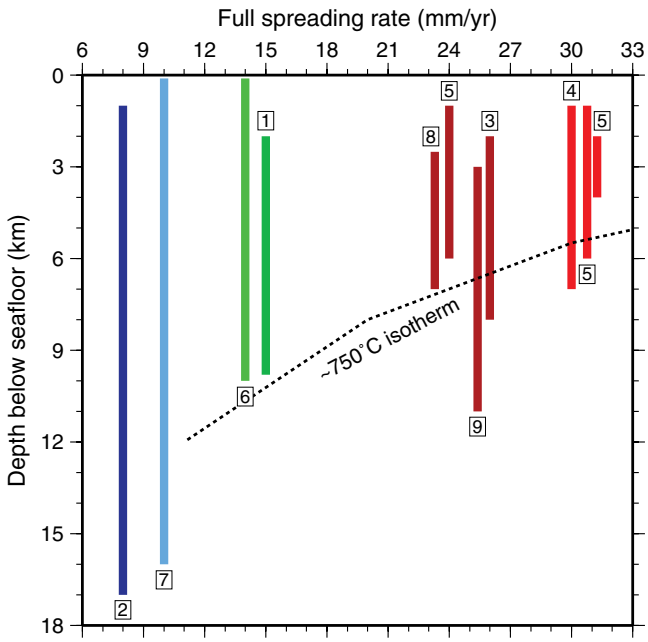

Figure 3. Compilation of depth distributions of micro-earthquakes as function of spreading rate, numbered as: 1—Mid-Cayman Spreading Center (this study); 2—Southwest Indian Ridge (SWIR) between 13°E and 14°E (this study); 3—Mid-Atlantic Ridge (MAR) at 29°N (Wolfe et al., 1995); 4—MAR at 5°S (Tilmann et al., 2004); 5—MAR at 14°75′N–7°15′S and 7°30′–8°S (Grevemeyer et al., 2013); 6—SWIR at 69°–70°E (Katsumata et al., 2001); 7—Gakkel Ridge (Arctic Ocean) at 85°E (Korger and Schlindwein, 2014); 8—MAR at 26°N (deMartin et al., 2007); 9—MAR 13°30′N (Parnell-Turner et al., 2017).

the hypocenter location procedure that did not include a thickness of few hundred meters of unconsolidated sediment. Once this sediment is included, a focal depth range of 1–17 km results, and the overall pattern of relocated events is very similar to that observed along other ultraslow-spreading ridges (Fig. 3). However, we note that 17 km maximum depth of microearthquakes at the SWIR is still deeper than observed along the MCSC (Fig. 1). We suggest that the greater maximum depth of seismicity simply reflects the lower effective spreading rate. The spreading rate of 15 mm/yr at the MCSC is only slightly faster than 11.2 mm/yr at the SWIR, but, if its obliquity is considered, the SWIR effective spreading rate is much lower at ~8 mm/yr (Dick et al., 2003). This may suggest that a decreased effective spreading rate with high associated obliquity mechanically affects increasingly deeper levels of the lithosphere to, or even below, the brittle-ductile transition. Furthermore, microseismicity may occur within a region defined by the seafloor and the maximum depth of faulting, supporting the hypothesis that temperature is the primary factor controlling the rheology of the oceanic lithosphere (Searle and Escartín, 2004) rather than lithology and hydration (Schlindwein and Schmid, 2016).

However, an alternative interpretation is that differences in the maximum depth of seismicity are, instead, related to temporal variations in spreading process rather than spreading rate itself. In this case, phases of spreading dominated by magmatic activity, related to injection of melt into the shallow lithosphere, would lead to a high heat flux and, hence, higher lithospheric temperature. In contrast, magmatically starved phases would be dominated by tectonic extension with faulting extending to a greater depth, thus promoting mining of heat by circulating fluids and resulting in a cooler lithosphere.

At the MCSC, seafloor spreading accompanied by magmatic activity clearly occurred during accretion of the relatively thick (~5 km) crust under the Mount Dent oceanic core complex (Harding et al., 2017) and distributed basaltic crust within the median valley (Van Avendonk et al., 2017; Haughton et al., 2019). However, both within the axial rift as well as off axis, large domains are characterized by serpentinized mantle exposed at the seafloor (e.g., Hayman et al., 2011), suggesting that the style of spreading has repeatedly switched, over time and in position along axis, between magma-rich and magma-poor oceanic crustal accretion (Grevemeyer et al., 2018b). On this basis, it is reasonable to hypothesize that seismicity extending to greater depth may characterize phases of little magma and heat flux into the lithosphere and, hence, a deep-seated brittle-to-plastic transition. In contrast, higher magmatic and heat flux may increase lithospheric temperature, causing a shallower brittle-to-plastic transition zone and, in turn, shallower seismicity. Yet, even at its most robust, magmatic accretion at the MCSC has been below global average rates (Harding et al., 2017; Van Avendonk et al., 2017). Consequently, the detachment faulting observed on the eastern flank of the Mount Dent oceanic core complex could result in anomalously deep seismicity, such as that observed at some oceanic core complexes along the MAR (deMartin et al., 2007; Parnell-Turner et al., 2017).

In conclusion, spreading rate, phases of magma-poor seafloor spreading, and deeply rooted detachment faulting may all affect and control the maximum depth of faulting along mid-ocean ridges, such that it is not necessary to invoke pervasive serpentinization and hydration to create a regime of shallow aseismic creep and deep seismicity along ultraslow-spreading centers.

ACKNOWLEDGMENTS

We thank the officers, engineers, and crew of the F/S *Meteor* for their support during the M115 CAYSEIS cruise. This project was funded by the UK's Natural Environment Research Council (NERC) (grant NE/K011162/1), the U.S. National Science Foundation (NSF) (grant OCE-1356895), and the German Research Foundation (DFG). Seismic data were recorded with instruments provided by University of Texas Institute for Geophysics and Helmholtz Centre for Ocean Research Kiel (GEOMAR), as well as the NERC's Ocean-Bottom Instrumentation Facility (Minshull et al., 2005). Hayman was serving as a Program Director at the NSF during preparation of this manuscript. The manuscript benefitted from constructive reviews from Rob Sohn, Tim Reston, and an anonymous reviewer.

REFERENCES CITED

Chen, W.-P., and Molnar, P., 1983, Focal depths of intracontinental and intraplate earthquakes and their implications for the thermal and mechanical properties of the lithosphere: Journal of Geophysical Research, v. 88, p. 4183–4214, https://doi.org/10.1029/JB088iB05p04183.

Connelly, D.P., et al., 2012, Hydrothermal vent fields and chemosynthetic biota on the world's deepest seafloor spreading centre: Nature Communications, v. 3, 620, https://doi.org/10.1038/ncomms1636.

deMartin, B.J., Sohn, R.A., Canales, J.P., and Humphris, S.E., 2007, Kinematics and geometry of active detachment faulting beneath the Trans-Atlantic Geotraverse (TAG) hydrothermal field on the Mid-Atlantic Ridge: Geology, v. 35, p. 711–714, https://doi.org/10.1130/G23718A.1.

Dick, H.J.B., Lin, J., and Schouten, H., 2003, An ultraslow-spreading class of ocean ridge: Nature, v. 426, p. 405–412, https://doi.org/10.1038/nature02128.

Grevemeyer, I., Reston, T.J., and Moeller, S., 2013, Microseismcity of the Mid-Atlantic Ridge at 7°–8°15′S and at the Logatchev Massif oceanic core complex at 14°40′N–14°50′N: Geochemistry Geophysics Geosystems, v. 14, p. 3532–3554, https://doi.org/10.1002/ggge.20197.

Grevemeyer, I., Ranero, C.R., and Ivandic, M., 2018a, Structure of oceanic crust and serpentinization at subduction trenches: Geosphere, v. 14, p. 395–418, https://doi.org/10.1130/GES01537.1.

Grevemeyer, I., Hayman, N.W., Peirce, C., Schwardt, M., Van Avendonk, H.J.A., Dannowski, A., and Papenberg, C., 2018b, Episodic magmatism and serpentinized mantle exhumation at an ultraslow-spreading centre: Nature Geoscience, v. 11, p. 444–448, https://doi.org/10.1038/s41561-018-0124-6.

Harding, J.L., Van Avendonk, H.J.A., Hayman, N.W., Grevemeyer, I., and Peirce, C., 2017, Magmatic-tectonic conditions for hydrothermal venting on an ultraslow-spread oceanic core complex: Geology, v. 45, p. 839–842, https://doi.org/10.1130/G39045.1.

Huang, P.Y., and Solomon, S.C.,1988, Centroid depths of mid-ocean ridge earthquakes: dependence on spreading rate: Journal of Geophysical Research, v. 93, p. 13445–13477, https://doi.org/10.1029/JB093iB11p13445.

Haughton, G.A., Hayman, N.W., Searle, R.C., Le Bas, T., and Murton, B.J., 2019, Volcanic-tectonic structure of the Mount Dent oceanic core complex in the ultraslow Mid-Cayman Spreading Center determined from detailed seafloor investigation: Geochemistry Geophysics Geosystems, v. 20, p. 1298–1318, https://doi.org/10.1029/2018GC008032.

Hayman, N.W., Grindlay, N.R., Perfit, M.R., Mann, P., Leroy, S., and de Lépinay, B.M., 2011, Oceanic core complex development at the ultraslow spreading Mid-Cayman Spreading Center: Geochemistry, Geophysics, Geosystems, v. 12, Q0AG02, https://doi.org/10.1029/2010GC003240.

Horning, G., Sohn, R.A., Canales, J.P., and Dunn, R.A., 2018, Local seismicity of the Rainbow massif on the Mid-Atlantic Ridge: Journal of Geophysical Research: Solid Earth, v. 123, p. 1615–1630, https://doi.org/10.1002/2017JB015288.

Katsumata, K., Sato, T., Kasahara, J., Hirata, N., Hino, R., Takahashi, N., Sekine, M., Miura, S., Koresawa, S., and Wada, N., 2001, Microearthquake seismicity and focal mechanisms at the Rodriguez Triple Junction in the Indian Ocean using ocean bottom seismometers: Journal of Geophysical Research, v. 106, p. 30,689–30,699, https://doi.org/10.1029/2000JB000106.

Klein, E.M., and Langmuir, C.H., 1987, Global correlations of ocean ridge basalt chemistry with axial depth and crustal thickness: Journal of Geophysical Research, v. 92, p. 8089–8115, https://doi.org/10.1029/JB092iB08p08089.

Kong, L.S.L., Solomon, S.C., and Purdy, G.M., 1992, Microearthquake characteristics of a mid-ocean ridge along-axis high: Journal of Geophysical Research, v. 97, p. 1659–1685, https://doi.org/10.1029/91JB02566.

Korger, E.I.M., and Schlindwein, V., 2014, Seismicity and structure of the 85°E volcanic complex at the ultraslow spreading Gakkel Ridge from local earthquake tomography: Geophysical Journal International, v. 196, p. 539–551, https://doi.org/10.1093/gji/ggt390.

Lefeldt, M., Grevemeyer, I., Goßler, J., and Bialas, J., 2009, Intraplate seismicity and related mantle hydration at the Nicaraguan trench outer rise: Geophysical Journal International, v. 178, p. 742–752, https://doi.org/10.1111/j.1365-246X.2009.04167.x.

Lomax, A., Virieux, J., Volant, P., and Berge-Thierry, C., 2000, Probabilistic earthquake location in 3D and layered models: Introduction of a Metropolis-Gibbs method and comparison with linear locations, in Thurber, C.H. and Rabinowitz, N., eds., Advances in Seismic Event Location: Amsterdam, Kluwer, p. 101–134, https://doi.org/10.1007/978-94-015-9536-0_5.

Minshull, T.A., Sinha, M.C., and Peirce, C., 2005, Multi-disciplinary, sub-seabed geophysical imaging: A new pool of 28 seafloor instruments in use by the United Kingdom Ocean Bottom Instrument Consortium: Sea Technology, v. 46, p. 27–31.

Morgan, J.P., and Chen, Y.J., 1993, The genesis of oceanic crust: Magma injection, hydrothermal circulation, and crustal flow: Journal of Geophysical Research, v. 98, p. 6283–6297, https://doi.org/10.1029/92JB02650.

Parnell-Turner, R., Sohn, R.A., Peirce, C., Reston, T.J., MacLeod, C.J., Searle, R.C., and Simão, N.M., 2017, Oceanic detachment faults generate compression in extension: Geology, v. 45, p. 923–926, https://doi.org/10.1130/G39232.1.

Schlindwein, V., and Schmid, F., 2016, Mid-ocean-ridge seismicity reveals extreme types of ocean lithosphere: Nature, v. 535, p. 276–279, https://doi.org/10.1038/nature18277.

Schmid, F., and Schlindwein, V., 2016, Microearthquake activity, lithospheric structure, and deformation modes at an amagmatic ultraslow spreading Southwest Indian Ridge segment: Geochemistry Geophysics Geosystems, v. 17, p. 2905–2921, https://doi.org/10.1002/2016GC006271.

Searle, R.C., and Escartín, J., 2004, The rheology and morphology of oceanic lithosphere and mid-ocean ridges, *in* German, C.R., et al., eds., Mid-Ocean Ridges: Hydrothermal Interactions Between the Lithosphere and Oceans: American Geophysical Union Geophysical Monograph 148, p. 63–93, https://doi.org/10.1029/148GM03.

Sohn, R.A., Fornari, D.J., Von Damm, K.L., Hildebrand, J.A., and Webb, S.C., 1998, Seismic and hydrothermal evidence for a cracking event on the East Pacific Rise crest at 9°50′ N: Nature, v. 396, p. 159–161, https://doi.org/10.1038/24146.

Tilmann, F., Flueh, E., Planert, L., Reston, T., and Weinrebe, W., 2004, Microearthquake seismicity of the Mid-Atlantic Ridge at 5°S: A view of tectonic extension: Journal of Geophysical Research, v. 109, B06102, https://doi.org/10.1029/2003JB002827.

Van Avendonk, H.J.A., Hayman, N.W., Harding, J.L., Grevemeyer, I., Peirce, C., and Dannowski, A., 2017, Seismic structure and segmentation of the axial valley of the Mid-Cayman Spreading Center: Geochemistry Geophysics Geosystems, v. 18, p. 2149–2161, https://doi.org/10.1002/2017GC006873.

Wolfe, C.J., Purdy, G.M., Toomey, D.R., and Solomon, S.C., 1995, Microearthquake characteristics and crustal velocity structure at 29°N on the Mid-Atlantic Ridge: The architecture of a slow spreading segment: Journal of Geophysical Research, v. 100, p. 24,449–24,472, https://doi.org/10.1029/95JB02399.

Printed in USA